

Imaging ultra-compact objects with radiative inefficient accretion flows

Saurabh^{1,2,*}, Parth Bambhaniya^{2,**} and Pankaj S. Joshi^{2,***}

¹ Max-Planck-Institut für Radioastronomie, Auf dem Hügel 69, D-53121 Bonn, Germany

² International Centre for Space and Cosmology, School of Arts and Sciences, Ahmedabad University, Ahmedabad-380009, Gujarat, India

ABSTRACT

Context. Recent Event Horizon Telescope observations of M87* and Sgr A* strongly suggests the presence of supermassive black hole at their respective cores. In this work, we use the semi-analytic Radiatively Inefficient Accretion Flows (RIAF) model to investigate the resulting images of Joshi-Malafarina-Narayan (JMN-1) naked singularity and the Schwarzschild BH.

Aims. We aim at choosing the JMN-1 naked singularity model and compare the synchrotron images with the Schwarzschild solution to search any distinct features which can distinguish the two objects and find alternative to the black hole solution.

Methods. We perform general relativistic ray-tracing and radiative transfer simulations using Brahma code to generate synchrotron emission images utilising thermal distribution function for emissivity and absorptivity. We investigate effects in the images by varying inclination angle, disk width and frequency.

Results. The shadow images simulated by the JMN-1 model closely resemble those generated by the Schwarzschild black hole. When we compare these images, we find that the disparities between them are minimal. We conduct simulations using various plasma parameters, but the resulting images remain largely consistent for both scenarios. This similarity is evident in the horizontal cross-sectional brightness profiles of the two instances. Notably, the JMN-1 model exhibits slightly higher intensity in comparison to the Schwarzschild black hole.

Conclusions. We conclude that JMN-1 presents itself as a viable substitute for the black hole scenario. This conclusion is not solely grounded in the fact that they are indistinguishable from their respective shadow observations, but also in the consideration that JMN-1 emerges as an end state of a continual gravitational collapse. This paradigm not only allows for constraints on spacetime but also provides a good probe for the nature of the central compact object.

Key words. Black hole physics; Radiative transfer; Accretion, accretion disks.

1. Introduction

In 1939, Oppenheimer, Snyder, and Datt (Oppenheimer & Snyder 1939) derived the first dynamical collapse solution for a spherically symmetric and homogeneous dust cloud, which later became known as OSD collapse. Their groundbreaking work demonstrated that a spherically symmetric and homogeneous dust collapse inevitably leads to the formation of a Schwarzschild black hole (BH). This result aligns with Birkhoff's theorem, which states that the Schwarzschild spacetime represents the most general vacuum solution of Einstein's equations. However, the OSD collapse model relies on several idealized assumptions, such as the homogeneity of the collapsing star's density, the neglect of gas pressure, and no rotation, to simplify the complex Einstein equations (Joshi & Malafarina 2011). Although this model unveils the development of an event horizon during the collapse, preventing the escape of matter, particles, or light to distant observers, it necessitates the exploration of more realistic scenarios that go beyond these idealistic assumptions. By considering the physical complexities and incorporating fac-

tors like non-homogeneous density profiles and gas pressure, we can expand our understanding of gravitational collapse and its implications.

Large astrophysical bodies typically do not possess a homogeneous density profile throughout their structure. Instead, their density can vary, with higher density at the core and decreasing values towards the surface. When considering more physically realistic scenarios, introducing inhomogeneity into the matter distribution profile and accounting for non-zero pressures, the dynamical collapse can result in the formation of a strong curvature singularity within the framework of general relativity (Joshi & Malafarina 2011; Joshi & Dwivedi 1993; Joshi et al. 2011; Janis et al. 1968; Mosani et al. 2020, 2021). The final states of such collapses depend on the initial conditions of the collapsing matter.

The general theory of relativity predicts that spacetime singularities necessarily form when sufficiently massive objects collapse under their own gravity. However, the simultaneous formation, or absence, of an event horizon is not enforced. A singularity that forms without an event horizon is known as a naked or cosmic singularity. Naked singularities are intriguing, horizonless compact objects characterized by ultra-high density regions, where physical quantities diverge arbitrarily. This ultra-dense compact region can be described by models of various astrophysical compact objects, e.g., the BH, naked singularity (NS), boson star, and others (Joshi & Malafarina 2011; Joshi &

* sbhkmr1999@gmail.com

* Member of the International Max Planck Research School (IMPRS) for Astronomy and Astrophysics at the Universities of Bonn and Cologne

** grcollapse@gmail.com

*** psjcosmos@gmail.com

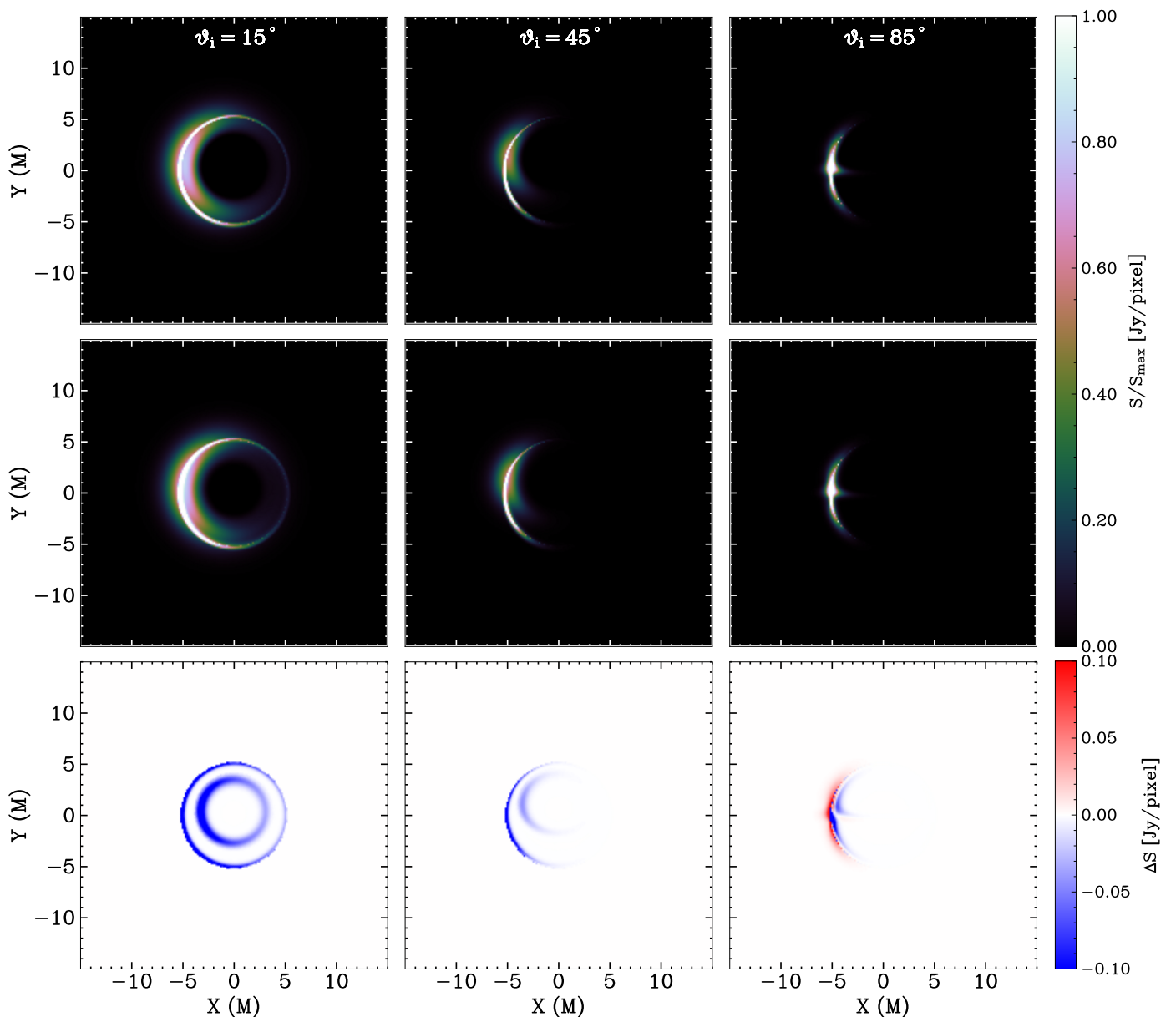


Fig. 1: Model images for Schwarzschild BH (first row) and the JMN-1 model (second row) for varied inclination angle (θ_{obs}). The third row corresponds to the various differences of images of second row from the first row.

Dwivedi 1993; Joshi et al. 2011; Janis et al. 1968; Schunck & Mielke 2003). These compact objects have fascinating physical and geometrical properties, and it would be observationally significant to distinguish them.

The cosmic censorship conjecture (CCC), proposed by Penrose (Penrose 1965), posits that strong horizonless singularities are prohibited. However, several research studies have revealed the potential formation of naked singularities during continuous gravitational collapses of inhomogeneous matter clouds. In a seminal work, Joshi, Malafarina, and Narayan (JMN) (Joshi et al. 2011) demonstrated that a non-zero tangential pressure can prevent the formation of trapped surfaces around the high-density core of a collapsing matter cloud, leading to the emergence of a central NS in extended co-moving time. This NS, occurring in physically realistic astrophysical scenarios, holds significant observational consequences. It gives rise to captivating phenomena such as distorted shadows, intense gravitational

lensing, and orbital precession of nearby stars (Vagnozzi et al. 2023; Sahu et al. 2012; Bambhaniya et al. 2022a).

On the other hand, black holes have astonishing features as well. As its distinct signature, a black hole possesses an event horizon, a one-way membrane in spacetime where things can fall in but not escape away and even light cannot escape. Almost every galaxy is thought to have a supermassive black hole at its core (Kormendy & Ho 2013). There is, however, no conclusive proof at this time for the existence of an event horizon. The Event Horizon Telescope (EHT) captured the first shadow image in 2019 in the galaxy M87 (Event Horizon Telescope Collaboration et al. 2019), and more recently in the center of our own galaxy, SgrA*. (Event Horizon Telescope Collaboration et al. 2022). While these results are indeed exciting, the interpretation should be dealt with caution. For instance, Mizuno et al. (2018) and Röder et al. (2023) performed general relativistic magnetohydrodynamics (GRMHD) simulations of a dilaton

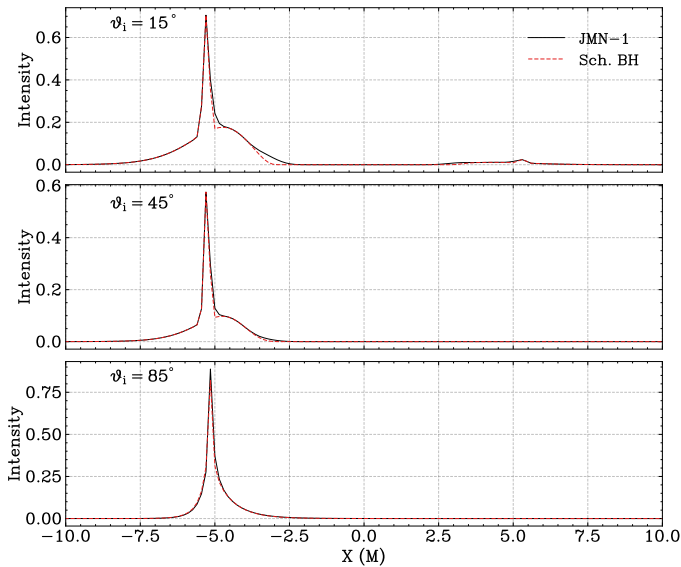


Fig. 2: Cross-sectional horizontal intensity for model images of Figure 1 with varied inclination angle (θ_{obs}).

BH and compared it with the Kerr BH, and concluded that it is difficult to distinguish them based on the shadow images alone. Additionally, many other such works hint towards the presence of such ‘mimickers’, therefore the shadow images of M 87* and Milky Way’s galactic centers observed by the EHT do not confirm the existence of an event horizon and hence a supermassive black hole (SMBH). Other compact objects can also cast similar shadows. The shadows cast by compact objects such as black holes, naked singularities, grava-stars, and wormholes have been extensively studied in Gralla et al. (2019); Vagnozzi & Visinelli (2019); Bambhaniya et al. (2022b); Gylchev et al. (2019); Atamurotov et al. (2015); Ohgami & Sakai (2015); Bambhaniya et al. (2021); Stuchlík & Schee (2019); Sakai et al. (2014); Solanki et al. (2022); Younsi et al. (2023).

It is generally believed that the shadows arise due to the presence of a photon sphere. Recently, however, in Joshi et al. (2020), the authors have introduced a new spherically symmetric NS solution of the Einstein field equation that lacks a photon sphere but nevertheless casts a shadow. The general criteria for a shadow to occur in the absence of a photon sphere are then determined for null and timelike naked singularities, where both types of singularities satisfy all the energy conditions Dey et al. (2021). Moreover, another model of NS which was proposed in 1968 by Janis-Newman-Winicour (JNW) can cast a shadow similar to that of a Schwarzschild black hole Gylchev et al. (2020); Sau et al. (2020). The JNW NS is a minimally coupled massless scalar field solution of the Einstein field equations. In Sau et al. (2020), the authors showed that as the scalar field charge q increases, the radius of the photon sphere r_{ph} increases while the shadow radius decreases.

In Shaikh et al. (2019), the shadows of Joshi-Malafarina-Narayan (JMN-1) NS spacetimes are investigated, and the results are compared to a Schwarzschild black hole shadow. For the range of the characteristic parameter $0 < M_0 < 2/3$, there is no photon sphere, and hence no shadow is formed in JMN-1 NS, yet an intriguing, full moon image is formed. However, JMN-1 can cast a shadow for $2/3 < M_0 < 1$, similar to that of a Schwarzschild black hole.

In this paper, we use a semi-analytic RIAF model to investigate the resulting images of JMN-1 and the Schwarzschild black

hole surrounded by accretion flows. Motivated by RIAF, we integrate the system of geodesics and the radiative transfer equation along them to compute the theoretical observed intensity.

The paper is organized as follows. In section (2), we briefly introduce the JMN-1 model. We describe the semi-analytic RIAF model in Section (3). In Section (4), we describe the ray-tracing formalism and the initial conditions we use to generate accretion images. In Section (5), we summarize our results. Finally, the discussion and conclusion are given in Section (6).

2. JMN-1 Naked Singularity

Here, we will briefly review the solution that have been proposed in the literature for the JMN-1 NS. The spacetime metric for a static and spherically symmetric object in the generalised form can be written as,

$$ds^2 = -g_{tt}(r)dt^2 + g_{rr}(r)dr^2 + g_{\theta\theta}(r)d\theta^2 + g_{\phi\phi}(r)d\phi^2, \quad (1)$$

where, $g_{\mu\nu}$ are the metric tensor components, all of which are only functions of r . The JMN-1 naked singularity can be formed as an end state of gravitational collapse with zero radial pressure and non-zero tangential pressures. These equilibrium configurations of the collapsing fluid within the general theory of relativity are extensively studied in Joshi et al. (2011). The JMN-1 naked singularity spacetime is described by the following metric tensor components,

$$g_{tt}^{jmn} = (1 - M_0) \left(\frac{r}{R_b} \right)^{M_0/(1-M_0)}, \quad (2)$$

$$g_{rr}^{jmn} = (1 - M_0)^{-1}, \quad (3)$$

$$g_{\theta\theta}^{jmn} = r^2, \quad (4)$$

$$g_{\phi\phi}^{jmn} = r^2 \sin^2 \theta, \quad (5)$$

where, M_0 and R_b are positive constants. Here, R_b represents the radius of the distributed matter around the central singularity and M_0 should be within the range $0 < M_0 < 1$. The JMN-1 spacetime contains a curvature singularity at $r = 0$. The stress-energy tensor of the JMN-1 spacetime gives the energy density ρ and pressures p as,

$$\rho = \frac{M_0}{r^2}, \quad p_r = 0, \quad p_\theta = \frac{M_0}{4(1 - M_0)}\rho. \quad (6)$$

Note that in JMN-1, the collapsing fluid is supported only by tangential pressure, and it can be verified that all the energy conditions are satisfied by this spacetime.

The spacetime metric is modeled by considering a high-density compact region in a vacuum, which means that the spacetime configuration should be asymptotically flat. Therefore, if any spacetime metric is not asymptotically flat, we must match that interior spacetime to an asymptotically flat exterior spacetime with a particular radius. The latter is the case for the JMN-1 naked singularity. We can smoothly match this interior spacetime to exterior Schwarzschild spacetime at $r = R_b$ as,

$$ds^2 = -\left(1 - \frac{M_0 R_b}{r}\right) dt^2 + \left(1 - \frac{M_0 R_b}{r}\right)^{-1} dr^2 + r^2 d\Omega^2, \quad (7)$$

where, $d\Omega^2 = d\theta^2 + \sin^2 \theta d\phi^2$ and $M = \frac{1}{2} M_0 R_b$ is the total mass of the compact object. The extrinsic curvatures of JMN-1 and Schwarzschild spacetimes are automatically smoothly matched at $r = R_b$, since the JMN-1 spacetime has zero radial pressure (Bambhaniya et al. 2019).

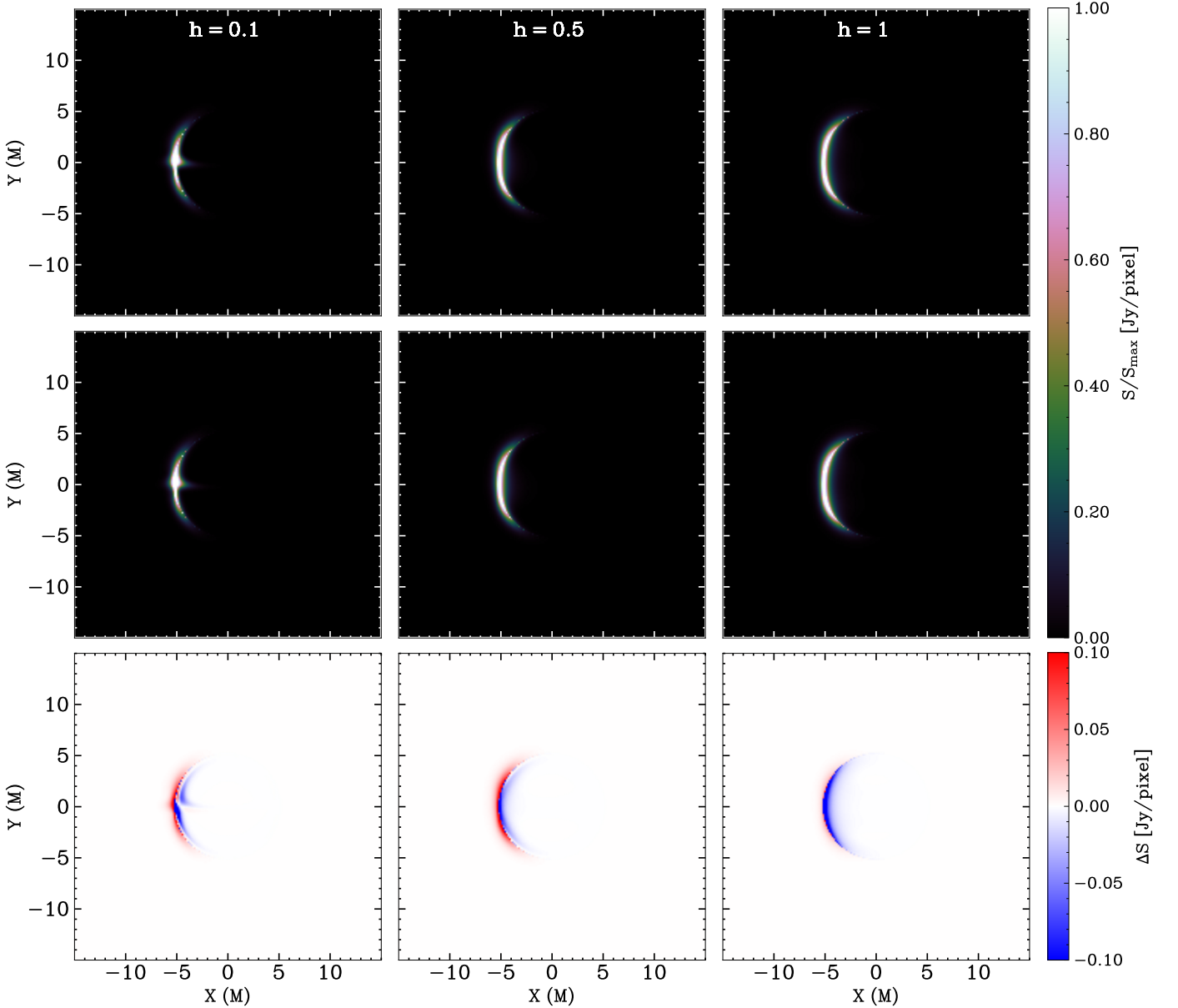


Fig. 3: Model images for Schwarzschild BH (first row) and the JMN-1 model (second row) for varied disk width (h). The third row corresponds to the different difference of images of second row from the first row.

3. Radiative Transfer

In this section, we describe the prescription for the semi-analytic radiative inefficient accretion flows (RIAF) model. We closely follow [Pu & Broderick \(2018\)](#) for some basic definitions of the parameters. The covariant form of general relativistic radiative transfer is expressed as

$$\frac{d\mathcal{I}}{d\tau_\nu} = -\mathcal{I} + \frac{\eta}{\chi}, \quad (8)$$

where \mathcal{I} is the Lorentz-invariant intensity and is related to the specific intensity via $\mathcal{I} = I_\nu/\nu^3 = I_{\nu_0}/\nu_0^3$ where the subscript ‘0’ denotes quantities in the local rest frame. τ_ν is defined as the optical depth. χ and η are the invariant absorption coefficient and emission coefficient at frequency ν . These coefficients are defined by the specific emissivity and absorptivity. For this work, we utilize the thermal electron distribution function (eDF) ([Pandya et al. 2016](#)).

The number density and temperature of electrons can be written as a hybrid combination of radial and exponential functions given by

$$n_{\text{th}} = n_{\text{e,th}} r^{-\alpha} e^{-z^2/2h^2}, \quad (9)$$

$$T_{\text{th}} = T_{\text{e,th}} r^{-\beta}, \quad (10)$$

where $z = r \cos \theta$ and h is the disk width. $n_{\text{e,th}}$ and $T_{\text{e,th}}$ are the respective normalization parameters. The magnetic field strength of the toroidal field is then given by

$$\frac{B^2}{8\pi} = \frac{1}{10} n_{\text{th}} \frac{m_p c^2}{6r}. \quad (11)$$

where $r_g = GM/c^2$ and m_p is the mass of proton.

We model the four-velocity of the plasma accreting onto the central compact object by following [Younsi et al. \(2023\)](#). The four-velocity can be written as

$$u^\mu = (u^t, u^r, 0, \Omega u^t). \quad (12)$$

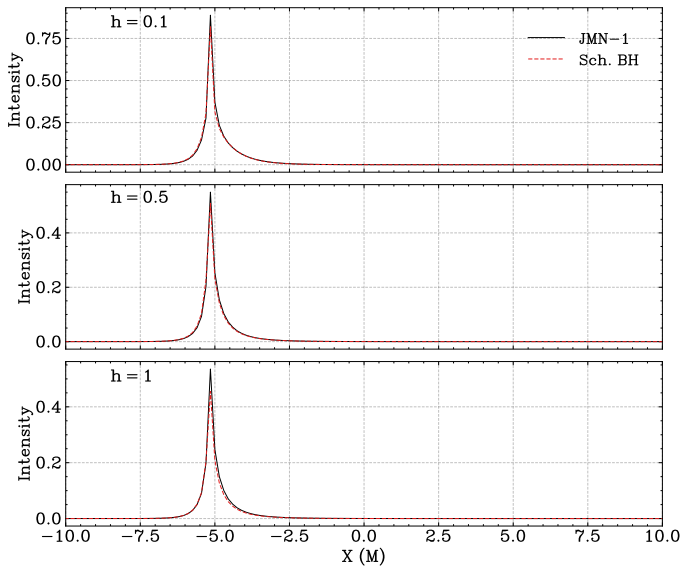


Fig. 4: Cross-sectional horizontal intensity for model images of Figure 3 with varied disk width (h).

where (Ω) is the angular velocity. The radial component of the four-velocity can be written in parameterized form,

$$u^r = -\eta_r \left(\frac{r}{R_{\text{ISCO}}} \right)^{-n_r}, \quad (13)$$

where $\eta_r = 0.1$ and $n_r = 1.5$ are the free parameters. We keep their values fixed for current analyses.

Since there are no stable circular orbits beyond the innermost stable circular orbit (ISCO) radius (r_{ISCO}), the particles will plunge with constant energy (E_{ISCO}) and constant angular momentum (L_{ISCO}) acquired at the ISCO radius. In this way, one can model the motion of particles for $r < r_{\text{ISCO}}$.

4. Ray-Tracing Formalism

In order to calculate the shadow image of a BH or naked singularity, one must first solve the geodesic equations in the considered background spacetime. To this end we use the *Brahma* code (*in preparation*). Here, we briefly describe the approach for ray-traced images of the models described in Section 3. We solve a system of 6 differential equations ($t, \dot{r}, \dot{\theta}, \dot{\phi}, \dot{p}_r, \dot{p}_\theta$).

4.1. Geodesic equations of motion

For a given metric $g_{\alpha\beta}$, the Lagrangian and the Hamiltonian can be written as

$$2\mathcal{L} = g_{\alpha\beta} \dot{x}^\alpha \dot{x}^\beta, \quad (14)$$

$$2\mathcal{H} = g^{\alpha\beta} p_\alpha p_\beta, \quad (15)$$

where an overdot denotes differentiation with respect to the affine parameter, λ . The corresponding equations of motion are given by

$$\dot{x}^\alpha = \frac{\partial \mathcal{H}}{\partial p_\alpha}, \quad (16)$$

$$\dot{p}_\alpha = -\frac{\partial \mathcal{H}}{\partial x^\alpha}. \quad (17)$$

From the Lagrangian, the covariant four-momenta of a geodesic may be written as:

$$p_\alpha = \frac{\partial \mathcal{L}}{\partial \dot{x}^\alpha}. \quad (18)$$

Using the conservation of energy and angular momentum, this can be broken down to write $p_t = -E$ and $p_\phi = L$ where E is the total energy of the particle and L is the angular momentum in the direction of ϕ . To solve the system of an ordinary differential equation (ODE), initial conditions are required. In the literature different authors have assumed different initial conditions based on the type of work and ODE's which are needed to be solved. In *Brahma*, we use the formalism described in [Younsi et al. \(2016\)](#). The observer is placed far away from the compact object ($r_{\text{obs}} = 10^3 M$), where the spacetime is assumed to be flat (asymptotic flatness).

5. Results

We use the formalism described in Section 4 to trace the photons along geodesics, and solve for the observed intensity. The model, in principle, consists of various parameters which can be altered to study specific properties of the accretion flows. In our simulations, we currently restrict ourselves to only a specific set of parameters $\Theta_p = (\theta_{\text{obs}}, \nu_{\text{obs}}, h)$. We study the impact of these parameters in the shadow images of both Schwarzschild BH and JMN-1 naked singularity. The default values for the parameters are: $\nu_{\text{obs}} = 230 \text{ GHz}$, $h = 0.1$, $n_{e,\text{th}} \approx 10^5 \text{ cm}^{-3}$ and $T_{e,\text{th}} \approx 10^{10} \text{ K}$.

- *inclination angle*: In Figure 1, the first row corresponds to the Schwarzschild BH, second row corresponds to the JMN-1 and the third row represents the image difference by subtracting second row images from the first row images. The first, second and third columns represents $\theta_{\text{obs}} = 15^\circ, 45^\circ$ and 85° respectively. Although both Schwarzschild BH and JMN-1 model images may look identical in terms of shadow features and emission, slight differences can be seen in the third row. Figure 2 represents the intensity along the horizontal cross-section of the images, and overall profile remains similar throughout the image except for minor changes.
- *disk width*: Figure 3 is same as Figure 1 except for the change in disk width h . The first, second and third column corresponds to $h = 0.1, 0.5$ and 1 respectively. Higher and lower values of h allows for a thicker and thinner flow geometry of the accreting matter, which would correspond to a transformation from a spherical-like flow to a disk-like flow. The inclination angle here set to 85° . For $h = 0.1$, a distinct disk-like geometry can be seen, but for the other it's not the case. Since we use a thermal eDF, the images are different compared to those presented in [Pu & Broderick \(2018\)](#). For different values of h , the images are very similar for the Schwarzschild BH and the JMN-1 model, and the corresponding horizontal cross-sectional section is shown in Figure 4. Here, it can be seen that profiles for both spacetimes are again similar with JMN-1 having slightly larger intensity for $h = 0.1$.
- *frequency*: Currently EHT operates at 230 GHz, and there are plans in action to include other frequency bands as part of EHT and nEHT. To this end, we also performed simulations for different frequencies as well, and the results are plotted in Figure 5 for 84 GHz, 230GHz, and 345 GHz. No significant changes are observed for the two spacetimes relative to each other when the observed frequency is changed. Although, as the frequency is increased the emission becomes thinner which is in agreement with previous results. The horizontal cross-sectional intensity as plotted in Figure 6 retains a similar profile as seen in previous cases for different values of disk width and inclination angle.

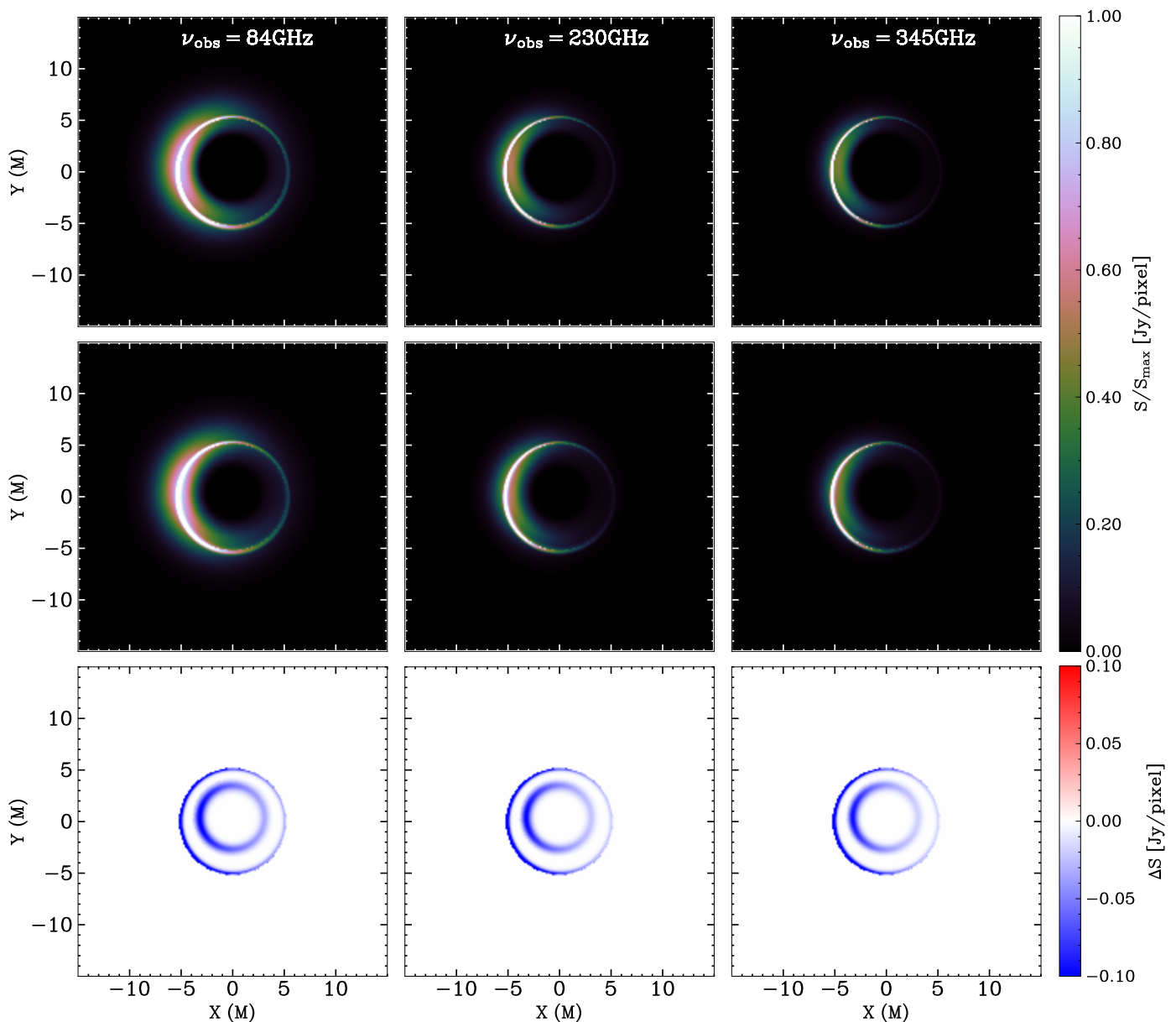


Fig. 5: Model images for Schwarzschild BH (first row) and the JMN-1 model (second row) for varied observed frequency (ν_{obs}). The third row corresponds to the different difference of images of second row from the first row.

6. Conclusion and Discussion

Here, we have modeled radiative inefficient accretion flows around JMN-1 cosmic singularity and calculated the resultant shadow images. Since JMN-1 results in a shadow of the same size as the Schwarzschild BH, it makes it worthwhile to investigate various effects from the change in spacetime, on the accretion flows and resultant images. We first define the geodesic equations for both photons and particles. We then define our semi-analytic RIAF model in Section 3. Thereafter, we solve the system geodesic equations with the raytracing formalism as described in Section 4 and simultaneously the radiative transfer equation to calculate the observed intensity. In order to compare the JMN-1 naked singularity with the Schwarzschild BH, we carry out simulations to generate images for various values of the parameters: inclination angle (θ_{obs}), disk width (h), and observed frequency (ν_{obs}). The results from the simulations are presented in Section 5.

The visual representations of both the Schwarzschild BH and JMN-1 model exhibit striking similarities, with subtle differences lying in the slightly heightened intensities observed in the JMN-1 model. Despite manipulating several parameters associated with the accretion disk, the overall characteristics of the disk remain relatively unchanged, reflecting the results of prior studies (Shaikh et al. 2019; Shaikh & Joshi 2019). Our results obtained here contribute to an expanded understanding of a realistic model for the accretion disk, which holds astrophysical relevance particularly in the context of AGNs. Following the fact that JMN-1 emerges as the end state of gravitational collapse, and acts as galactic spacetime, this opens up an intriguing avenue into the study of AGNs where the central engine powering the galaxy is a visible cosmic singularity. The above analysis concludes that if horizon-scale observations of the central supermassive compact object produces a shadow-like structure, differentiating between a BH and a naked singularity remains in-

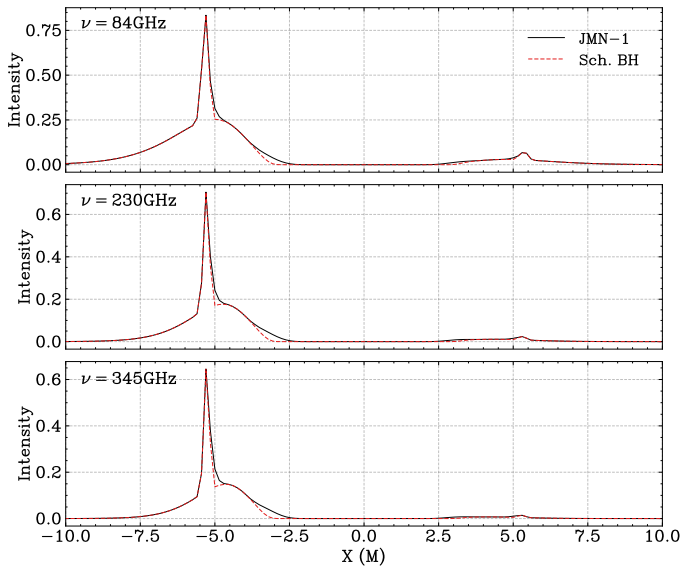


Fig. 6: Cross-sectional horizontal intensity for model images of Figure 5 with varied observed frequency (ν_{obs}).

discernible, and by extension to the recent studies of M 87* and Sgr A*.

However, there are many other paths that can be pursued further in order to test and investigate the robustness of the model. For example, we can generate synthetic VLBI observations from the ray traced images presented in this paper to be able to compare our results directly to observational data.

- For instance, [Shaikh et al. \(2019\)](#) have considered a spherically accreting system and studied their shadow images. Bondi accretion flow was also utilised to study shadow and spectral properties using MHD simulations. This type of treatment can also be applied to our model to study the spectra, which can then be used to study specific sources such as Sgr A*. Spectral signatures will be studied in an accompanying paper soon.
- We only studied the horizon-scale accretion flow images of the models, and in GRMHD simulations, black holes produce highly-energetic jets seen in various observations. Studies of jets and accretion flows in GRMHD simulations will help us to reach a conclusive result on the presence of horizon-less objects in the Universe.

Using the models described in this work, it will be possible to unveil the true nature of the objects in M 87* and Sgr A*. From the studies so far it would appear that naked singularities present a possible alternative to the standard picture of a black hole within the framework of non-modified general relativity.

Acknowledgements. Saurabh received financial support for this research from the International Max Planck Research School (IMPRS) for Astronomy and Astrophysics at the Universities of Bonn and Cologne. We would also like to acknowledge Jan Röder for his role as the internal referee at the MPIfR and helpful comments.

References

Atamurotov, F., Ahmedov, B., & Abdujabbarov, A. 2015, *Phys. Rev. D*, 92, 084005
 Bambhaniya, P., Dey, D., Joshi, A. B., et al. 2021, *Phys. Rev. D*, 103, 084005
 Bambhaniya, P., Joshi, A. B., Dey, D., & Joshi, P. S. 2019, *Phys. Rev. D*, 100, 124020

Bambhaniya, P., Joshi, A. B., Dey, D., et al. 2022a [arXiv:2209.12610]
 Bambhaniya, P., K, S., Jusufi, K., & Joshi, P. S. 2022b, *Phys. Rev. D*, 105, 023021
 Dey, D., Joshi, P. S., & Shaikh, R. 2021, *Phys. Rev. D*, 103, 024015
 Event Horizon Telescope Collaboration, Akiyama, K., Alberdi, A., et al. 2022, *ApJ*, 930, L12
 Event Horizon Telescope Collaboration, Akiyama, K., Alberdi, A., et al. 2019, *ApJ*, 875, L5
 Gralla, S. E., Holz, D. E., & Wald, R. M. 2019, *Phys. Rev. D*, 100, 024018
 Gylchev, G., Kunz, J., Nedkova, P., Vetsov, T., & Yazadjiev, S. 2020, *European Physical Journal C*, 80, 1017
 Gylchev, G., Nedkova, P., Vetsov, T., & Yazadjiev, S. 2019, *Phys. Rev. D*, 100, 024055
 Janis, A. I., Newman, E. T., & Winicour, J. 1968, *Phys. Rev. Lett.*, 20, 878
 Joshi, A. B., Dey, D., Joshi, P. S., & Bambhaniya, P. 2020, *Phys. Rev. D*, 102, 024022
 Joshi, P. S. & Dwivedi, I. H. 1993, *Phys. Rev. D*, 47, 5357
 Joshi, P. S. & Malafarina, D. 2011, *International Journal of Modern Physics D*, 20, 2641
 Joshi, P. S., Malafarina, D., & Narayan, R. 2011, *Classical and Quantum Gravity*, 28, 235018
 Kormendy, J. & Ho, L. C. 2013, *ARA&A*, 51, 511
 Mizuno, Y., Younsi, Z., Fromm, C. M., et al. 2018, *Nature Astronomy*, 2, 585
 Mosani, K., Dey, D., & Joshi, P. S. 2020, *Phys. Rev. D*, 101, 044052
 Mosani, K., Dey, D., & Joshi, P. S. 2021, *MNRAS*, 504, 4743
 Ohgami, T. & Sakai, N. 2015, *Phys. Rev. D*, 91, 124020
 Oppenheimer, J. R. & Snyder, H. 1939, *Physical Review*, 56, 455
 Pandya, A., Zhang, Z., Chandra, M., & Gammie, C. F. 2016, *ApJ*, 822, 34
 Penrose, R. 1965, *Phys. Rev. Lett.*, 14, 57
 Pu, H.-Y. & Broderick, A. E. 2018, *ApJ*, 863, 148
 Röder, J., Cruz-Ororio, A., Fromm, C. M., et al. 2023, *A&A*, 671, A143
 Sahu, S., Patil, M., Narasimha, D., & Joshi, P. S. 2012, *Phys. Rev. D*, 86, 063010
 Sakai, N., Saida, H., & Tamaki, T. 2014, *Phys. Rev. D*, 90, 104013
 Sau, S., Banerjee, I., & SenGupta, S. 2020, *Phys. Rev. D*, 102, 064027
 Schunck, F. E. & Mielke, E. W. 2003, *Classical and Quantum Gravity*, 20, R301
 Shaikh, R. & Joshi, P. S. 2019, *J. Cosmology Astropart. Phys.*, 2019, 064
 Shaikh, R., Kocherlakota, P., Narayan, R., & Joshi, P. S. 2019, *MNRAS*, 482, 52
 Solanki, D. N., Bambhaniya, P., Dey, D., Joshi, P. S., & Pathak, K. N. 2022, *Eur. Phys. J. C*, 82, 77
 Stuchlík, Z. & Schee, J. 2019, *European Physical Journal C*, 79, 44
 Vagnozzi, S. & Visinelli, L. 2019, *Phys. Rev. D*, 100, 024020
 Vagnozzi, S. et al. 2023, *Class. Quant. Grav.*, 40, 165007
 Younsi, Z., Psaltis, D., & Özel, F. 2023, *ApJ*, 942, 47
 Younsi, Z., Zhidenko, A., Rezzolla, L., Konoplya, R., & Mizuno, Y. 2016, *Phys. Rev. D*, 94, 084025